Silicon (2023) 15:8031–8043
https://doi.org/10.1007/s12633-023-02636-8

RESEARCH

Radiation Attenuation Properties of Zinc-Borosilicate Glasses Containing Al_2O_3 and Gd_2O_3

Nada Alfryyan[1] · Z. A. Alrowaili[2] · Sultan Alomairy[3] · Islam M. Nabil[4] · M. S. Al-Buriahi[5]

Received: 17 July 2023 / Accepted: 16 August 2023 / Published online: 1 September 2023

Abstract
This study explores the radiation shielding properties of an xGd_2O_3 – $(60\text{-}x)ZnO$–$15B_2O_3$–$5Al_2O_3$–$20SiO_2$ glass system (x = 0—3 mol %) glass system using FLUKA and XCOM software. The glass system is interesting due to its potential applications in nuclear and medical settings, where effective radiation-shielding materials are crucial. The FLUKA Monte Carlo simulation package is utilized to model the interaction of gamma photons with the glass system. At the same time, the XCOM software calculates the macroscopic cross-sections based on their elemental composition. The investigation evaluates parameters such as attenuation coefficients, dose rates, neutron cross-section, and stopping power for different radiation sources and energies. Various configurations are analyzed by varying the Gd_2O_3 concentrations in the present glass system to optimize shielding effectiveness. The results refer to the high radiation shielding potential of gamma rays and neutrons for the present glassy materials compared to previously studied shielding materials. The present study offers valuable insights into the radiation shielding properties of the studied glass system, facilitating the design and development of efficient radiation shielding materials for practical implementation in nuclear and medical industries.

Keywords Borosilicate Glass · Radiation attenuation · Shielding application · FLUKA

1 Introduction

Nuclear science finds extensive application in various sectors, including nuclear facilities, research reactors, agriculture, industry, and nuclear medicine. These diverse applications result in the emission of different types of radiation, which can pose risks to the environment, animals, and people. Consequently, numerous researchers are actively discovering improved materials for radiation attenuation and shielding purposes. The primary objective is to develop materials that effectively mitigate the harmful effects of radiation by acting as barriers between radioactive sources and the surrounding area or workers, thereby reducing exposure to potentially dangerous radiation.

Radiation and nuclear medicine are just a few technological fields where radioactive isotopes are finding more appealing applications today [1, 2]. The environment, animals, and people can all be harmed by radiation gamma, X-rays, and neutrons. Shielding material is well recognized for providing a barrier between a radioactive source and the surrounding area or workers to decrease exposure to hazardous radiation [3]. So, the importance of radiation-shielding materials has increased. Many authors are interested in discovering new glassy systems to use as promised radiation shielding materials [4–8]. This knowledge is applied to produce new materials with specific traits and characteristics suitable for various technological purposes [5–9]. It is generally accomplished using dense materials such as lead or concrete that obstruct or deflect radiation [10]. Other materials, such as boron, are used for neutron shielding [6]. Also, cement, gypsum, borate glass, polymers, and lead are being used for radiation

✉ Sultan Alomairy
mohsaa996@gmail.com

✉ M. S. Al-Buriahi
alburiahi@sakarya.edu.tr

[1] Department of Physics, College of Science, Princess Nourah bint Abdulrahman University, P.O. Box 84428, 11671 Riyadh, Saudi Arabia

[2] Department of Physics, College of Science, Jouf University, P.O. Box:2014, Sakaka, Saudi Arabia

[3] Department of Physics, College of Science, Taif University, P.O. Box 11099, Taif 21944, Saudi Arabia

[4] Physics Department, Faculty of Science, Fayoum University, Fayoum, Egypt

[5] Department of Physics, Sakarya University, Sakarya, Turkey

shielding purposes, either conventionally or in complex ways [11–13]. Several researchers have discussed numerous systems for experimental measurements and theoretical work using various software on how radiation interacts with these materials (e.g., FLUKA, MCNP, Phy-X, XCOM, and GEANT4) [14–19]. The need for a reduction in exposure rate, source type, space restrictions, and ultimate cost-effective analysis influences the selection of materials. For example, Al-Buriahi et al. studied the gamma-ray shielding performance of a MoO_3-TeO_2 glass system that showed a promising application in nuclear safety, whether in nuclear or medicine facilities [20]. Gokhan et al. synthesized Ytterbium (III) oxide-reinforced novel TeO_2– based glasses that are investigated through their optical, structural, physical, and thermal properties and their radiation shielding ability [21]. Moreover, different simulation codes were used to assess the linear attenuation coefficient, which is a major part to calculate the other gamma shielding parameters such as HVL, MFP, Zeff, etc. [22–25].

Recent research has investigated the influence of Gd_2O_3 on the elastic properties of zinc borotellurite glass [26]. The findings suggest that the elastic moduli of these glassy materials increase with increasing Gd_2O_3, leading to improved connectivity and compactness of the glass network. This enhanced connectivity is attributed to the solidification effects of Gd_2O_3. In a related study, Morshidy et al. [27] explored the incorporation of Gd_2O_3 as a co-dopant in a chromium borate glass system. The researchers observed that introducing Gd_2O_3 resulted in increased compactness of the glass network, as evidenced by higher experimental density measurements. The presence of Gd_2O_3 further reinforced the structural integrity of the glass, leading to improved mechanical properties. These investigations demonstrate the positive influence of Gd_2O_3 on the elastic ability and compactness of zinc boro-tellurite glass and chromium borate glasses. These findings contribute to understanding how Gd_2O_3 can be utilized to enhance the structural properties of glass materials, potentially opening up new possibilities for tailored applications in various fields.

Similarly, the scientific community has also shown keen interest in investigating the effect of Gd_2O_3 on the radiation shielding performance of TeO_2–ZnO–Nb_2O_5 glasses [28] and Sb_2O_3–PbO–B_2O_3 [29]. However, no study shows the impact of Gd_2O_3 on the radiation/gamma shielding ability of ZnO–$5Al_2O_3$–$15B_2O_3$–$20SiO_2$ glass system, which can be considered one of the most applicable glasses. Therefore, this point encouraged the authors to establish the present work to pave the way for developing advanced glass materials with enhanced performance for various practical applications.

2 Materials and Method

2.1 Materials

The ternary xGd_2O_3 – (60-x)ZnO–$15B_2O_3$–$5Al_2O_3$–20 SiO_2 glass system (x = 0—3 mol %) with a density range of 3.775—4.109 $g.cm^{-3}$ is deliberated to be tested using ϒ-rays, fast and thermal neutrons using the radiation shielding parameters (e.g., μ/ρ, μ, etc.). These investigated glass systems have been prepared as described in [30]. The elemental chemical compositions and densities of the prepared glass samples are specified in Table 1.

2.2 FLUKA Simulation

The radiation shielding simulations of the investigated glasses were conducted using the FLUKA Monte Carlo code. A mono-energetic point source with an energy range of 0.015—15 MeV was employed to simulate the transit of electrons, neutrons, and gamma photons, considering the physics interaction principles such as photoelectric (PEEI), Compton scattering (Com), and pair production processes (PP). To perform the simulations, precise data regarding source dimensions, source-to-detector distance, geometry, elemental chemical composition, and other parameters were incorporated into the FLUKA input files, as shown in Fig. 1. The experimental system encompassed six components: a radioactive source, primary gamma-ray collimator, cylinder

Table 1 Sample code and weight fraction (wt.%) of element present the prepared ZnO–Al_2O_3–B_2O_3–SiO_2-Gd_2O_3 glasses including their measured density

Sample	Chemical composition (mol%)	Composition in wt.%						Density (g/cm^3)
		B	O	Al	Si	Zn	Gd	
ZABSG1	60.0ZnO-$5Al_2O_3$-$15B_2O_3$-$20SiO_2$	4.24562	33.51028	3.53200	7.35303	51.35905	0.00000	3.775
ZABSG2	59.5ZnO-$5Al_2O_3$-$15B_2O_3$-$20SiO_2$-0.5Gd_2O_3	4.16892	33.11052	3.46819	7.22019	50.01090	2.02128	3.860
ZABSG3	59.0ZnO-$5Al_2O_3$-$15B_2O_3$-$20SiO_2$-1.0Gd_2O_3	4.09494	32.72494	3.40664	7.09206	48.71060	3.97083	3.909
ZABSG4	58.0ZnO-$5Al_2O_3$-$15B_2O_3$-$20SiO_2$-2.0Gd_2O_3	3.95458	31.99343	3.28988	6.84897	46.24370	7.66944	4.011
ZABSG5	57.0ZnO-$5Al_2O_3$-$15B_2O_3$-$20SiO_2$-3.0Gd_2O_3	3.82353	31.31040	3.18085	6.62200	43.94030	11.12292	4.109

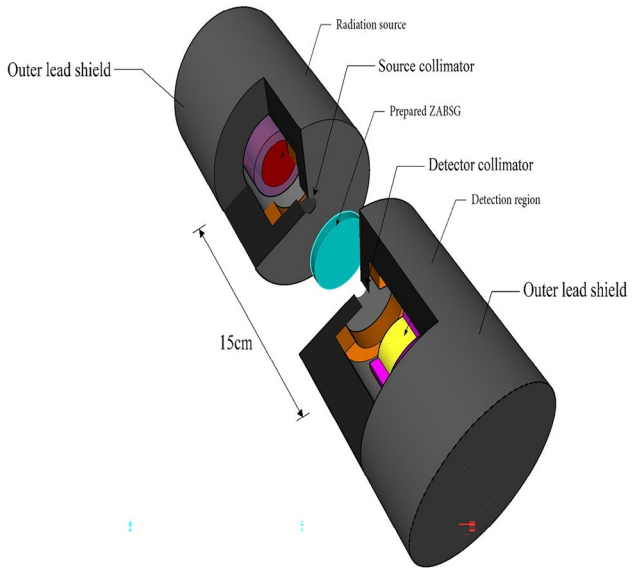

Fig. 1 FLUKA simulation setup used for evaluating the gamma-ray transmission parameters of the prepared ZABSG*x* glasses

sample, secondary gamma-ray collimator, detector, and an outer lead shield. The radioactive source was positioned within a lead collimator for primary gamma rays, with a radius of 0.14 cm and a height of 0.3 cm. It was located 15 cm away from the detector. A monoenergetic gamma-ray point source was defined for each input file in the energy range of 0.015—15 MeV. The samples under investigation were represented as cubic layers between the source and the detector. The material card contained information regarding the elemental composition and densities of the investigated xGd_2O_3 – (60-x) $ZnO–15B_2O_3–5Al_2O_3–20SiO_2$ glass samples. The detector was configured within a lead collimator for secondary gamma rays. The simulations were conducted with an outer lead shield surrounding the detector, source, collimators, and samples.

2.3 XCOM Software

The X-Com software is a web-based program that calculates many different factors associated with shielding and attenuation for the compositions of materials and dosimetry that have been investigated [31]. The mass attenuation coefficients (μm) were among the many numbers calculated from the XCOM input file. The input parameters include the elemental makeup and the energy ranges. To determine the relative differences (Dev., %) between the XCOM and FLUKA results, Dev. (%) = (FLUKA- XCOM)/(FLUKA) × 100.

2.4 Gamma Ray's Attenuation

Shielding materials can be identified by measuring their mass attenuation coefficient, which can be determined via the Lambert–Beer's law equation as follows [29]:

$$I = I_o e^{-\mu x}, \tag{1}$$

Where I is the intensity of transmitted gamma through the material, I_o is the intensity of primary gamma in air, x is the attenuator thickness, and μ is the linear attenuation coefficient. A valuable indicator of a material's characteristic as a radiation attenuator is the mass attenuation coefficient (μ_m) which could be calculated using the formula below [31]:

$$\mu_m = \frac{\mu}{\rho}, \tag{2}$$

where, w_i denotes the weight fraction of i^{th}-element in the studied materials. The $^{\mu}{}_{L}$ parameter is necessary to calculate the values needed to reduce the primary irradiation to half or a tenth of its original value. The following equations can be used to calculate the attenuator thickness, known as the half-value layer (*HVL*), to reduce the strength of the photon by half its original value [3, 4]:

$$HVL = \frac{ln2}{\mu}, \tag{3}$$

The average distance gets through by a photon before it interacts with the attenuator substance is known as the mean free path (λ) using Eq. 4 [22–26]:

$$\lambda = \frac{1}{\mu}, \tag{4}$$

The effective atomic number (Z_{eff}) is also a significant parameter for the materials under investigation as an attenuator and the effective electron density N_{eff}. To get the Z_{eff} for a material, the atomic cross section (*ACS* (σ_a)) and electronic cross section (*ECS* (σ_e)) are initially determined. The following equations can be used to determine these parameters as follows [22, 23, 32, 33]:

$$ACS = \sigma_a = \sigma_m \frac{1}{\sum_i n_i} = (\mu/\rho)_{target}/N_A \sum_i \frac{w_i}{A_i}, \tag{5}$$

where, w_i is the fractional weight of the target individual element, A_i is the atomic weight, σ_m is the molecular cross-section, and N_A is Avogadro's constant. Additionally, the following formula can be used to determine *ECS* as follows [32–35]:

$$ECS = \sigma_e = \frac{1}{N_A} \sum_i \left(\frac{\mu}{\rho}\right)_i \frac{f_i A_i}{z_i}, \tag{6}$$

The target individual element's fractional abundance is represented by f_i, and Z_i is the atomic number. So, Z_{eff} could be calculated as follows [36]:

Table 2 Mass attenuation coefficient of the prepared ZnO–Al_2O_3–B_2O_3–SiO_2-Gd_2O_3 glasses via FLUKA and XCOM at different photon energies

Energy (MeV)	ZABSG1			ZABSG2			ZABSG3		
	XCOM	FLUKA	Dev.%	XCOM	FLUKA	Dev.%	XCOM	FLUKA	Dev.%
0.015	43.36539	43.23413	0.303	44.13146	43.91802	0.484	44.87034	44.60053	0.601
0.02	19.85432	19.89412	0.200	20.22264	20.25274	0.149	20.57789	20.60874	0.150
0.03	6.47799	6.49688	0.292	6.61096	6.62821	0.261	6.73921	6.75224	0.193
0.04	2.93109	2.93563	0.155	2.99591	2.99929	0.113	3.05843	3.06118	0.090
0.05	1.60931	1.60693	0.148	1.64653	1.64222	0.262	1.68243	1.67590	0.388
0.06	1.00811	1.00592	0.217	1.22044	1.21891	0.126	1.42523	1.42367	0.110
0.08	0.51562	0.51666	0.203	0.61578	0.61662	0.135	0.71239	0.71370	0.184
0.1	0.33284	0.33337	0.159	0.38791	0.38854	0.164	0.44102	0.44146	0.100
0.15	0.18664	0.18676	0.065	0.20480	0.20486	0.029	0.22231	0.22243	0.051
0.2	0.14303	0.14380	0.536	0.15121	0.15191	0.460	0.15910	0.15972	0.392
0.3	0.11029	0.11079	0.453	0.11291	0.11338	0.416	0.11544	0.11578	0.295
0.4	0.09514	0.09534	0.209	0.09629	0.09644	0.155	0.09739	0.09751	0.123
0.5	0.08549	0.08574	0.292	0.08608	0.08625	0.201	0.08664	0.08681	0.204
0.6	0.07843	0.07830	0.154	0.07875	0.07861	0.175	0.07905	0.07891	0.178
0.8	0.06834	0.06846	0.177	0.06844	0.06853	0.130	0.06853	0.06864	0.157
1.0	0.06121	0.06098	0.374	0.06123	0.06098	0.406	0.06124	0.06098	0.420
1.5	0.04982	0.04952	0.592	0.04978	0.04949	0.597	0.04975	0.04944	0.617
2	0.04326	0.04301	0.588	0.04325	0.04299	0.604	0.04324	0.04297	0.615
3	0.03607	0.03574	0.902	0.03612	0.03579	0.909	0.03617	0.03584	0.914
4	0.03231	0.03201	0.934	0.03242	0.03212	0.926	0.03252	0.03222	0.921
5	0.03010	0.02985	0.850	0.03026	0.03000	0.852	0.03041	0.03015	0.842
6	0.02873	0.02852	0.708	0.02892	0.02872	0.705	0.02911	0.02891	0.696
8	0.02728	0.02714	0.510	0.02754	0.02740	0.497	0.02779	0.02765	0.492
10	0.02668	0.02656	0.447	0.02700	0.02688	0.440	0.02730	0.02718	0.433
15	0.02652	0.02643	0.355	0.02694	0.02684	0.350	0.02734	0.02725	0.332

Energy (MeV)	ZABSG4			ZABSG5		
	XCOM	FLUKA	Dev.%	XCOM	FLUKA	Dev.%
0.015	46.27212	45.91177	0.779	47.58099	47.18871	0.824
0.02	21.25186	21.28863	0.173	21.88115	21.90798	0.123
0.03	6.98253	6.99448	0.171	7.20972	7.22107	0.157
0.04	3.17704	3.17725	0.007	3.28779	3.28609	0.051
0.05	1.75054	1.73895	0.662	1.81413	1.79805	0.887
0.06	1.81376	1.81242	0.074	2.17654	2.17526	0.059
0.08	0.89568	0.89736	0.188	1.06682	1.06888	0.193
0.1	0.54178	0.54192	0.026	0.63586	0.63586	0.000
0.15	0.25554	0.25565	0.041	0.28657	0.28652	0.015
0.2	0.17407	0.17472	0.373	0.18804	0.18853	0.262
0.3	0.12023	0.12052	0.240	0.12471	0.12495	0.194
0.4	0.09949	0.09956	0.070	0.10144	0.10148	0.034
0.5	0.08770	0.08782	0.130	0.08870	0.08876	0.074
0.6	0.07964	0.07947	0.215	0.08019	0.07999	0.243
0.8	0.06871	0.06879	0.115	0.06887	0.06892	0.071
1.0	0.06126	0.06099	0.447	0.06128	0.06099	0.483
1.5	0.04969	0.04931	0.767	0.04963	0.04924	0.772
2	0.04321	0.04294	0.637	0.04319	0.04291	0.642
3	0.03626	0.03593	0.911	0.03635	0.03600	0.954
4	0.03272	0.03243	0.888	0.03290	0.03261	0.879

Table 2 (continued)

Energy (MeV)	ZABSG4			ZABSG5		
	XCOM	FLUKA	Dev.%	XCOM	FLUKA	Dev.%
5	0.03069	0.03043	0.845	0.03096	0.03070	0.834
6	0.02947	0.02926	0.687	0.02980	0.02959	0.686
8	0.02827	0.02813	0.480	0.02871	0.02857	0.471
10	0.02787	0.02775	0.432	0.02841	0.02829	0.416
15	0.02811	0.02801	0.335	0.02882	0.02873	0.334

$$Z_{eff} = \frac{\sigma_a}{\sigma_e}, \tag{7}$$

Build-up factors (*BUFs)* are important metrics demonstrating photon dispersion in radiation attenuation applications. We have to measure two parameters, *R* ratio, and Z_{eq}, to determine the (*BUFs)* [32–36]:

$$R = \frac{\left(\mu/\rho\right)_{Com}}{\left(\mu/\rho\right)_{Total}}, \tag{8}$$

where, $\left(\mu/\rho\right)_{Com}$ is the Compton μ_m and $\left(\mu/\rho\right)_{Total}$ is the total μ_m for the target or attenuator. When materials absorb photons, a virtual atomic number (Z_{eff}) describes the complex substance; this value is known as Z_{eq} when photons are scattered. The following formula can be used to compute the build-up factors' second key parameter (Z_{eq}) [32–36]:

$$Z_{eq} = \frac{Z_1\left(\log R_2 - \log \mathrm{R}\right) + Z_2\left(\log \mathrm{R} - \log \mathrm{R}_1\right)}{\log R_2 - \log R_1}, \tag{9}$$

The two types of buildup factors (*BUFs)* are Energy Absorption Buildup Factor (*EABF*) and Exposure Buildup Factor (*EBF*). By understanding the (*R)* and (Z_{eq}) parameters, one can calculate the geometric progression's (G-P) fitting parameters to compute the (*BUFs*) [36]:

$$P = \frac{P_1(\log Z_2 - \log Z_{eq}) + P_1(\log Z_{eq} - \log Z_1)}{\log Z_2 - \log Z_1}, \tag{10}$$

Z_1 and Z_2's respective atomic numbers are represented by the GP fitting parameters P_1 and P_2, respectively. Then, employing GP-fitting to the following equations, *BUFs* were investigated:

$$\begin{aligned} B(E,X) &= 1 + \frac{b-1}{K-1}(K^x - 1) for\ K \neq 1, B(E,X) \\ &= 1 + (b-1)x\ K = 1, \end{aligned} \tag{11}$$

and,

$$K(E,X) = cx^a + d\frac{tanh(\frac{x}{Xk} - 2) - tanh(-2)}{1 - tanh(-2)} \text{for x} \leq 40, \tag{12}$$

where (a, b, c, xk, and d) are G-P fitting parameters, *E* is the energy photon, *x* is the penetration depth in λ, and *K*(*E*, *X*) is the dose-multiplicative factor.

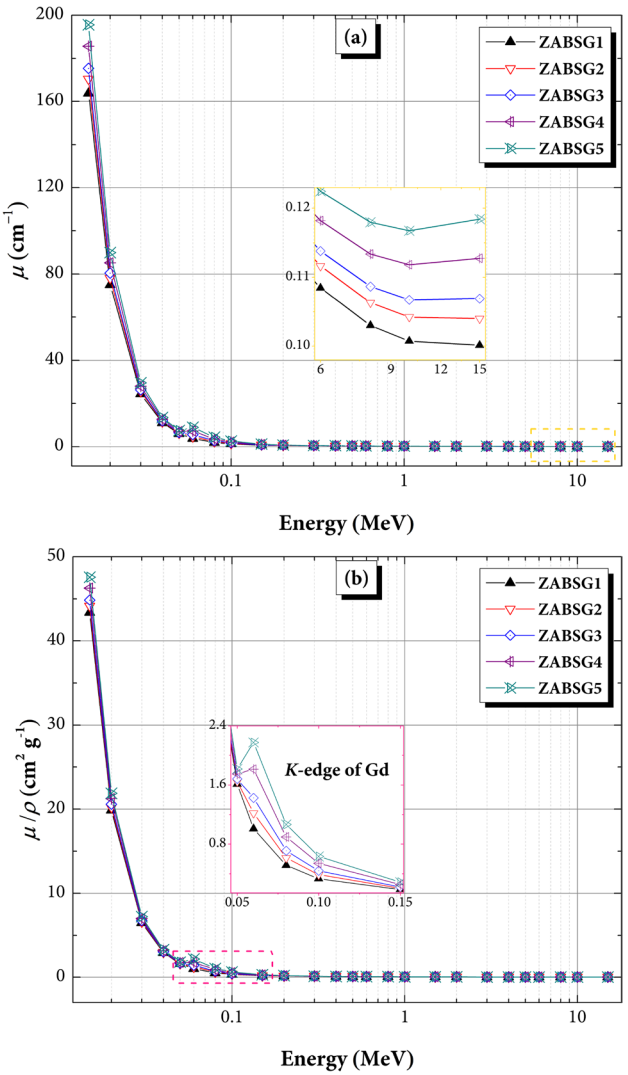

Fig. 2 (**a**) Linear attenuation coefficient (μ) and (**b**) mass attenuation coefficient (μ/ρ) of the prepared (60-*x*)ZnO–5Al_2O_3–15B_2O_3–20SiO_2–*x*Gd_2O_3 glasses (where *x* = 0, 0.5, 1, 2, and 3 mol%) with different photon energies

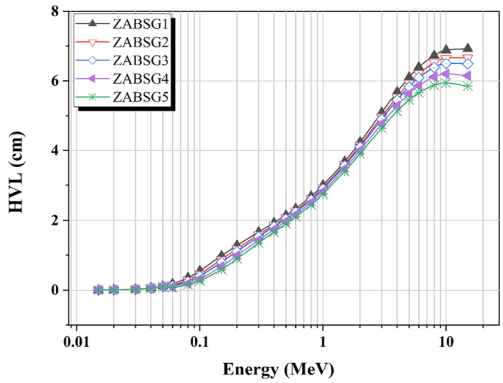

Fig. 3 Half value layer (HVL) with respect to the concentration of MoO_3 and a function of photon energy in the prepared (60-*x*)ZnO–5Al_2O_3–15B_2O_3–20SiO_2–*x*Gd_2O_3 glasses (where $x=0$, 0.5, 1, 2, and 3 mol%)

2.5 Neutron Rays Attenuation

The *FNRCS* (Σ_R) is a significant measure to evaluate the planned material systems' capacity for neutron attenuation. Knowing that the sample density represents by $(\rho)_s$, w_i is the i^{th}-ingredient weight fraction, W_i stands for partial density and $\left(\frac{\Sigma_R}{\rho}\right)_i$ is a representation of the ith component's mass removal cross-section, so any absorber's Σ_R can be calculated as follow [2, 5, 14, 15]:

$$\frac{\Sigma_R}{\rho} = \sum_i W_i \left(\frac{\Sigma_R}{\rho}\right)_i, \tag{13}$$

where,

$$W_i = \sum_i w_i(\rho)_s. \tag{14}$$

3 Results and Discussion

The μ/ρ values for the xGd_2O_3 – (60-x)ZnO–15B_2O_3–5Al_2O_3–20SiO_2 glass system (x = 0—3 mol %) were assessed using FLUKA and XCOM software to assess the radiation attenuation characteristics. The relative difference (Div. %) between the results obtained from FLUKA and XCOM are listed in the Table 2. The results showed good agreement

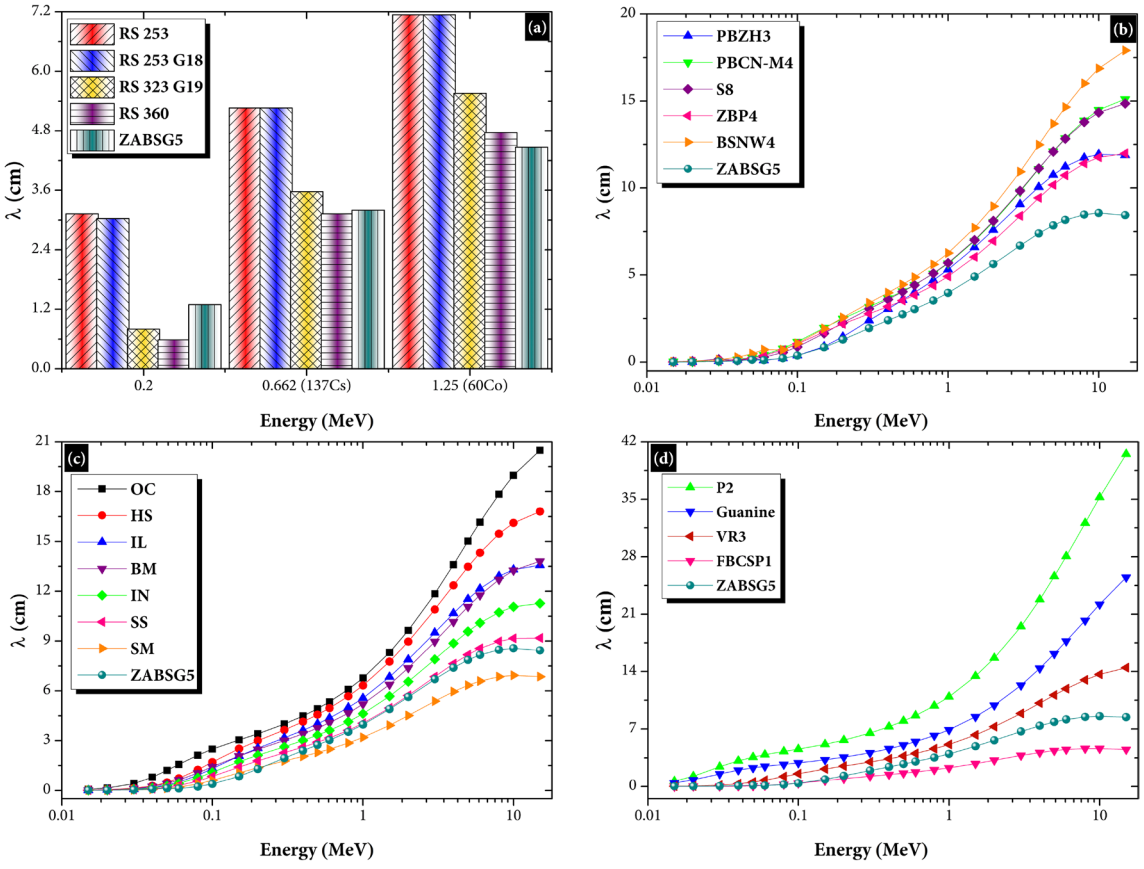

Fig. 4 Comparison of mean free path (λ) parameter of the prepared ZABSG5 sample with those in (**a**) commercial SCHOTT's radiation shielding glasses [1], (**b**) some glass systems [2–6], (**c**) standard shielding concretes [7], and (**d**) polymer-composite materials [8–11]

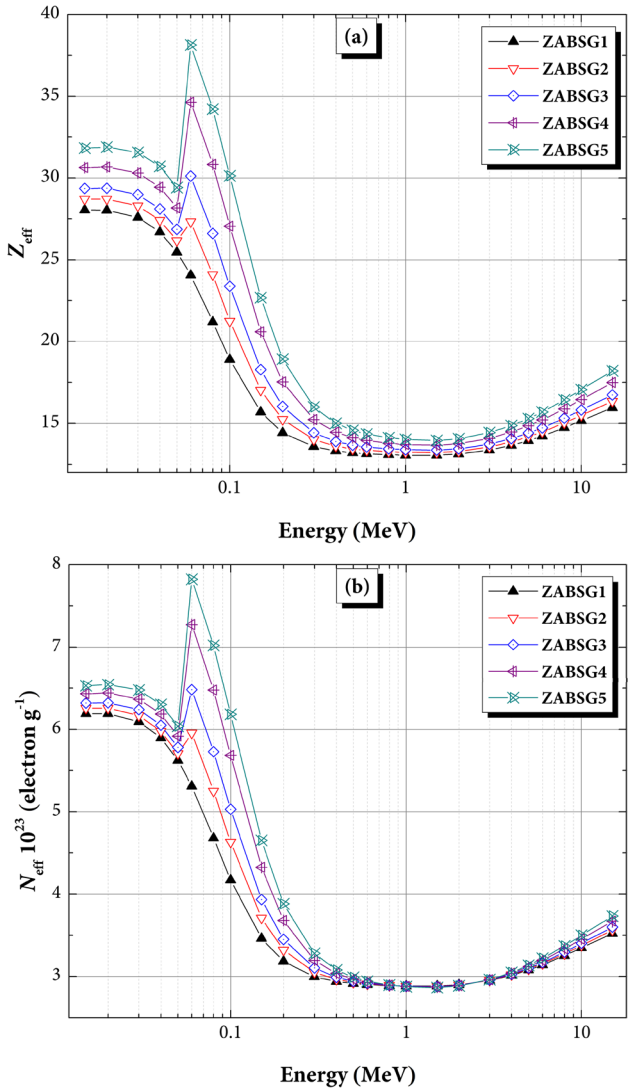

Fig. 5 **a** Effective atomic number and (**b**) effective electron density of the prepared (60-*x*)ZnO–5Al_2O_3–15B_2O_3–20SiO_2–*x*Gd_2O_3 glasses (where *x* = 0, 0.5, 1, 2, and 3 mol%), with different photon energies

with a maximum relative difference of 0.9540%. On the other hand, Fig. 2(b) represents that there is a strong reduction in the μ/ρ values for all prepared samples due to Photo electric effect interaction (PEEI) which has cross-section changes with $E_\gamma^{-3.5}$. Therefore, the interaction cross-section reduced strongly with the enrichment of photon values which is associated with a similar reduction in the photon-electron interactions and μ_L values. The enrichment of the applied E_γ values between 0.015–0.2 MeV causes a strong exponential decrease in the values of μ/ρ ($cm^2.g^{-1}$) trends from 43.2341 to 0.1438 for ZABSG1, from 43.9180 to 0.1512 for ZABSG2, from 44.60053 to 0.15972 for ZABSG3, from 45.9117 to 0.1747 for ZABSG4 and from 47.1887 to 0.1885 for ZABSG5. Furthermore, the enrichment of E_γ values above 0.2 MeV causes an exponential decrease in the μ/ρ values in the E_γ interval of 0.2 to 2 MeV. The exponential reduction is attributed to the Compton scattering interaction (Com) with cross-section changes with E_γ^{-1}. Photons with more kinetic energy have a lower probability of interacting with atoms in the substance [15]. Therefore, the probability of absorption decreases associated with the increased probability of photons scattering with increasing energy. The enrichment in E_γ values was associated with a smooth decrease in the cross-section with decreases in the number of photon-electron interactions followed by a smooth reduction in the μ/ρ values. There is a reduction in the μ/ρ values (in the unit of $cm^2.g^{-1}$) from 0.1107 to 0.0430 for ZABSG1, from 0.1133 to 0.0429 for ZABSG2, from 0.1157 to 0.0429 for ZABSG3, from 0.1205 to 0.0429 for ZABSG4 and from 0.1249 to 0.0429 for ZABSG5 with raising the E_γ values between 0.3 MeV and 2 MeV, respectively. Also, there is a little reduction due to the pair production interaction (PP) with cross-section changes with E_γ^2. The μ/ρ values, in this region vary from 0.0357 to 0.0264 for ZABSG1, from 0.0357 to 0.0268 for ZABSG2, from 0.0358 to 0.0272 for ZABSG3, from 0.0359 to 0.0280 for ZABSG4 and from 0.0360 to 0.0287 for ZABSG5 with raising the E_γ values between 3—15 MeV. The $\mu_{/\rho}$ values for ZABSG5 are generally the highest among the other prepared materials due to the high concentration of gadolinium element (11.1229%). Figure 2(a) shows The linear attenuation coefficient (μ, cm^{-1}) of the prepared samples, which take the same behavior as the $\mu_{/\rho}$ for the investigated samples. The μ values of ZABSG5 have higher than ZABSG1, ZABSG2, ZABSG3, and ZABSG4 at the same energy energies.

The half-value layer (HVL, cm) values for the synthetic Gd_2O_3 glass samples are displayed in Fig. 3 for various energies between 0.015—15 MeV**.** The HVL values for the studied samples increase as the energy of the radiation increases, which is expected. It's the thickness of the investigated samples that can shield half of the incident gamma photons. At lower and mid energy ranges (0.015 – 0.2 MeV), there are significant differences in the HVL values among the studied materials, but these differences decrease at the higher energies (0.3 – 2 MeV) and (3 – 15 MeV). The HVL values ranged from 0.00423 To 6.9236 cm for ZABSG1, from 0.0040 to 6.6660 for ZABSG2, from 0.0039 to 6.4853 cm for ZABSG3, from 0.0037 to 6.1483 for ZABSG4 and from 0.0035 to 5.8528 cm for ZABSG5 in the energy of 0.015 – 15 MeV. It suggests that ZABSG5 has the lowest values of HVL and may be better suited for radiation shielding.

Mean free path (ƛ) is a standard measure of radiation protection effectiveness. It also demonstrates whether or not the shielding material is of sufficient thickness. Since radiation is dampened by traveling through a thinner region, the lower values for either parameter often result in higher radiation shielding performance for a given photon energy. Typically, the ƛ all go up and down in tandem. Figure 4(a-d)

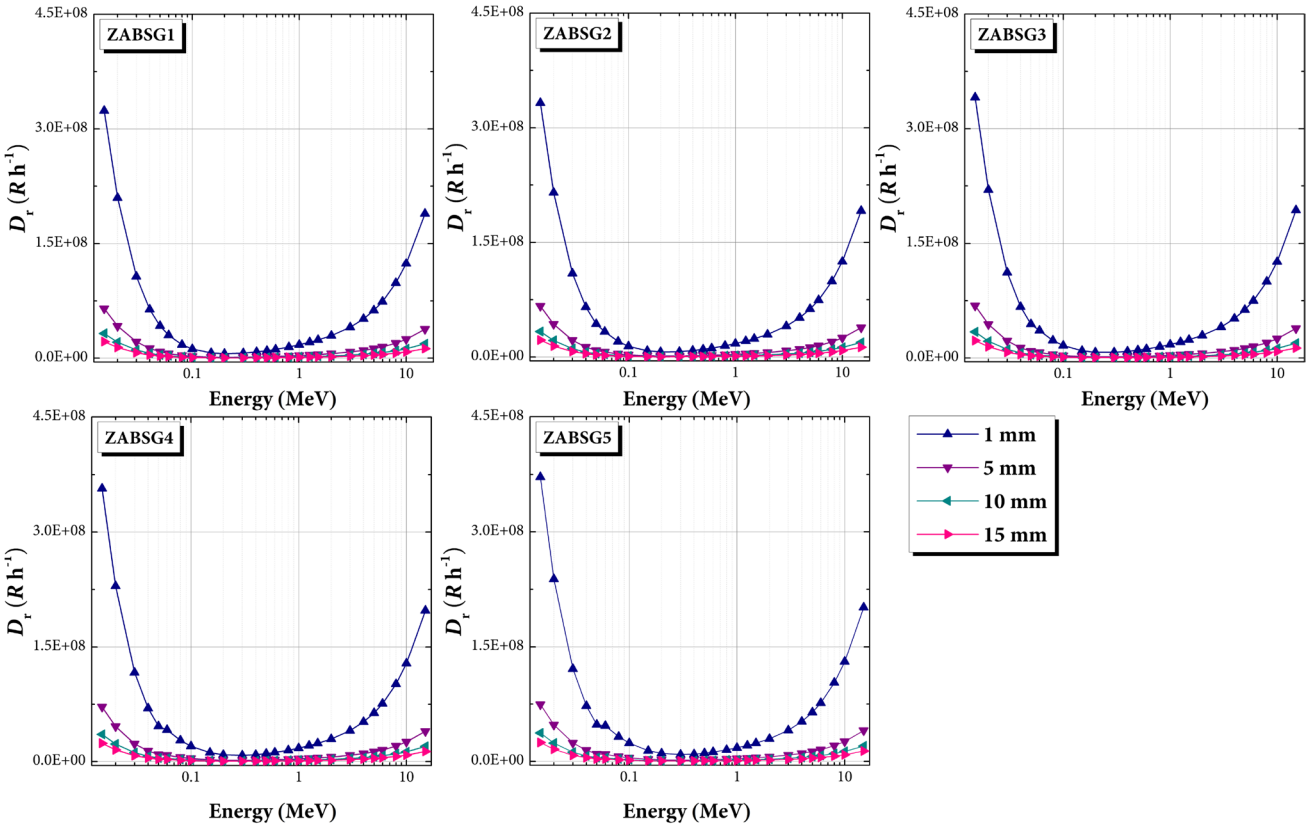

Fig. 6 Gamma dose rate (D_r) at different photon energy levels for the prepared (60-x)ZnO–5Al_2O_3–15B_2O_3–20SiO_2–$x$$Gd_2O_3$ glasses (where x = 0, 0.5, 1, 2, and 3 mol%)

compares the best-prepared sample ZABSG5 with those of different standard materials (e.g., SCHOTT's radiation shielding glasses (https://www.schott.com/en-gb), (b) some glass systems [37–41], (c) standard shielding concretes [10], and (d) polymer-composite materials [42–44]. Figure 4(a, b) show that the investigated ZABSG5 sample has the lowest values of ƛ with those of commercial SCHOTT's glass (RS-253, RS-253-G18, RS-323-G19, RS-360, and other glass samples) at photon energy 1.25 MeV. On the contrary, the ZABSG5 sample has a value higher than RS-323-G19 and RS-360 glass samples at photon energy 0.2 MeV.

Also, the investigated ZABSG5 glass sample has the lowest values of ƛ with all the compared standard concrete, Ordinary concrete (OC), Hematite-serpentine concrete (H–S), Ilmenite limonite concrete (IL), Basalt-magnetite concrete (B-M), Ilmenite concrete (IN) and Steel-scrap concrete (S–S) except the Steel magnetite (S-M) as shown in Fig. 4(c). Figure 4(d) shows that the prepared ZABSG5 sample has the lowest values of ƛ with those of polymer-composite (P2, Guanine, and VR3) except for the FBCSP1 sample.

Figure 5(a, b) presents the investigated glass samples' atomic effective number (Z_{eff}) values and effective electron

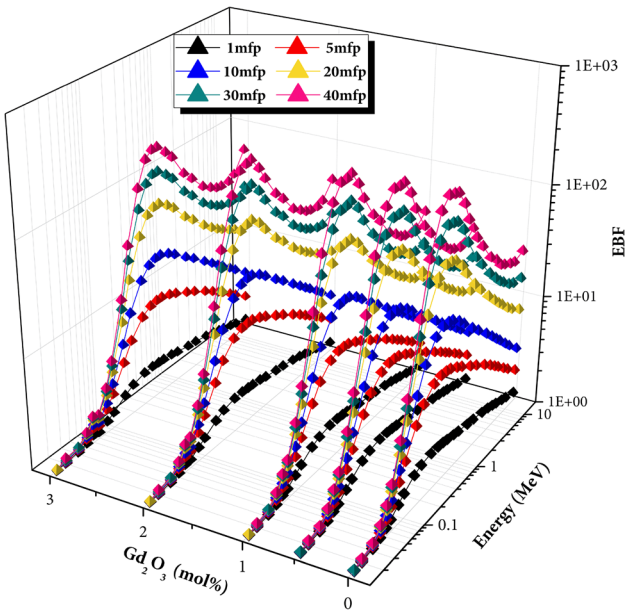

Fig. 7 Exposure buildup factor (EBF) with the photon energy for the prepared (60-x)ZnO–5Al_2O_3–15B_2O_3–20SiO_2–$x$$Gd_2O_3$ glasses (where x = 0, 0.5, 1, 2, and 3 mol%)

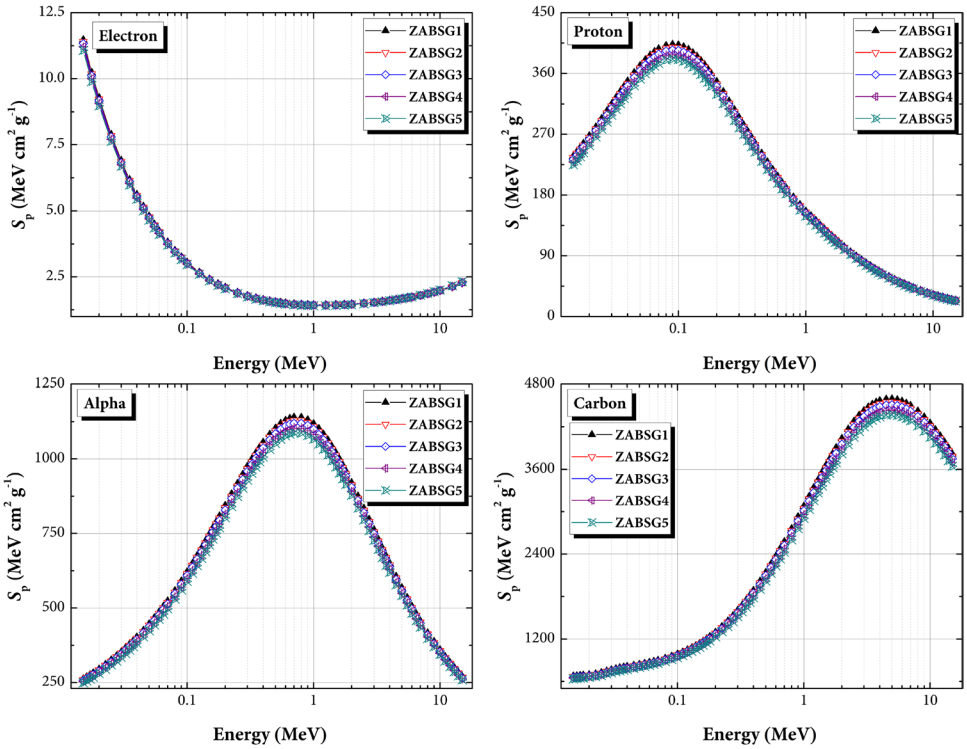

Fig. 8 Total mass stopping power with respect to a function of kinetic energy in the prepared (60-*x*)ZnO–5Al_2O_3–15B_2O_3–20SiO_2–*x*Gd_2O_3 glasses (where $x=0$, 0.5, 1, 2, and 3 mol%) presented for electron, proton & alpha particles, and carbon ion

density (N_{eff}) vs. photon energy in the energy range of 0.015 – 15 MeV. In general, the higher Z_{eff} and N_{eff} values indicate a greater ability of a material to interact with radiation, particularly through the Com and PEEI regions [45]. Therefore, materials with higher Z_{eff} values may be more effective in shielding against high-energy radiation. It indicates that the effectiveness of the materials in attenuation against radiation is dependent on the energy of the radiation and that a different material may be more effective at higher or lower MeV energy. At lower MeV values between 0.015—0.2, the ZABSG5 has the highest Z_{eff} *and* N_{eff} values among the four materials. As the MeV value increases, the Z_{eff} values for the studied materials decrease, but ZABSG5 still has the highest Z_{eff} and N_{eff} values. Also, the ZABSG1 compound has the lowest Z_{eff} values among the four materials.

Figure 6 displays the (60-x) ZnO–5Al_2O_3–15B_2O_3–20 SiO_2–xGd_2O_3 glass systems' computed gamma dose rate (D, R.h^{-1}) spectra outside glasses with thicknesses ranging from 1—15 mm. D's energy-dependent fluctuations at the various thicknesses under consideration show that gamma dose rate constant (C) has a significant impact on the variation. D also

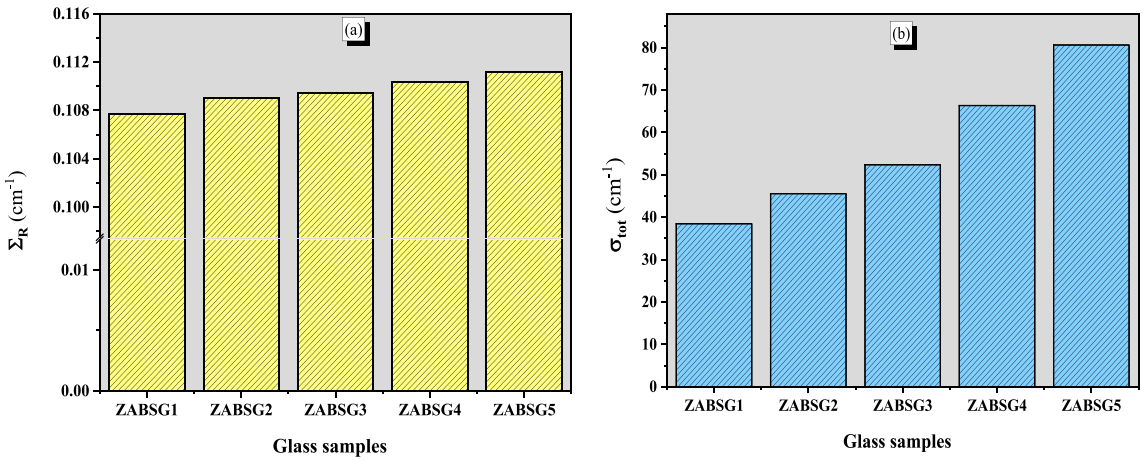

Fig. 9 (**a**) Removal (Σ_R), and (**b**) total scattering (σ_{tot}) cross sections of the prepared (60-*x*)ZnO–5Al_2O_3–15B_2O_3–20SiO_2–*x*Gd_2O_3 glasses (where $x=0$, 0.5, 1, 2, and 3 mol%) for fast and thermal neutrons

Table 3 Fast neutron removal cross-section of elements contained in the prepared ZnO–Al_2O_3–B_2O_3–SiO_2-Gd_2O_3 glasses

Glass code	Element	Σ_R/ρ (cm^2/g)	Fraction by weight, w_i	Partial density (g/cm^3), W_i	Σ_R (cm^{-1})
ZABSG1	B	0.05746705	0.0424562	0.16027231	0.00921038
	O	0.04052824	0.3351028	1.26501322	0.05126876
	Al	0.02934486	0.0353200	0.13333313	0.00391264
	Si	0.02814153	0.0735303	0.27757704	0.00781144
	Zn	0.01829517	0.5135905	1.93880429	0.03547076
	Gd	0.01192390	0.0424562	0.00000000	0.00000000
				$\Sigma_{R=}$	0.10767398
	Total Σ_R for glass 'ZABSG1'$_=$ **0.10767** cm^{-1}				
ZABSG2	B	0.05746705	0.0416892	0.16092029	0.00924761
	O	0.04052824	0.3311052	1.27806593	0.05179776
	Al	0.02934486	0.0346819	0.13387220	0.00392846
	Si	0.02814153	0.0722019	0.27869928	0.00784302
	Zn	0.01829517	0.5001090	1.93042080	0.03531738
	Gd	0.01192390	0.0202128	0.07802151	0.00093032
				$\Sigma_{R=}$	0.10906456
	Total Σ_R for glass 'ZABSG2'$_=$ **0.10906** cm^{-1}				
ZABSG3	B	0.05746705	0.0409494	0.16007109	0.00919881
	O	0.04052824	0.3272494	1.27921780	0.05184445
	Al	0.02934486	0.0340664	0.13316573	0.00390773
	Si	0.02814153	0.0709206	0.27722854	0.00780163
	Zn	0.01829517	0.4871060	1.90409728	0.03483579
	Gd	0.01192390	0.0397083	0.15521955	0.00185082
				$\Sigma_{R=}$	0.10943923
	TotalΣ_R for glass 'ZABSG3'$_=$ **0.10944** cm^{-1}				
ZABSG4	B	0.05746705	0.0395458	0.15861820	0.00911532
	O	0.04052824	0.3199343	1.28325638	0.05200812
	Al	0.02934486	0.0328988	0.13195705	0.00387226
	Si	0.02814153	0.0684897	0.27471226	0.00773082
	Zn	0.01829517	0.4624370	1.85483473	0.03393452
	Gd	0.01192390	0.0766944	0.30762139	0.00366805
				$\Sigma_{R=}$	0.11032909
	Total Σ_R for glass 'ZABSG4'$_=$ **0.11033** cm^{-1}				
ZABSG5	B	0.05746705	0.0382353	0.15710866	0.00902857
	O	0.04052824	0.3131040	1.28654442	0.05214138
	Al	0.02934486	0.0318085	0.13070124	0.00383541
	Si	0.02814153	0.0662200	0.27209788	0.00765725
	Zn	0.01829517	0.4394030	1.80550707	0.03303206
	Gd	0.01192390	0.1112292	0.45704073	0.00544971
				$\Sigma_{R=}$	0.11114438
	Total Σ_R for glass 'ZABSG5'$_=$ **0.11114** cm^{-1}				

varies negatively with glass thickness at all energy levels and types of glass. When the glass thickness and the photon energy remain constant, D varies negatively with Z_{eff}. The EBF and EABF values of the examined compounds fluctuate with photon energy at 1,—40 ƛ, as shown in Fig. 7. The photon energy, sample composition, and penetration depth influence the maximum values of the BUF. Multiple scatterings happen at greater penetration depths. The highest BUFs values were found at a penetration depth of 40 MFPs, and the lowest were found at a penetration depth of 1. The values of the BUFs rise with photon energy to their maximum value before falling as photon energy rises. The PEEI dominates interactions in the lower energy area; hence many photons have been absorbed, resulting in the lowest BUFs. Due to the prevailing

Com, which scatters the photon's energy but cannot destroy it, the region of intermediate photon energy has the highest BUFs values. The photons were once more absorbed in the higher energy region where pair formation is the dominant interaction. Figure 8(a-d) The electron, proton, alpha, and carbon mass stopping power (E/P/A/CS_P) and calculated range values of (60-x)ZnO–5Al2O3–15B2O3–20SiO2–xGd2O3 glasses were calculated by using FLUKA code. The MS_P results are important as they indicate the relation of the electron, proton, alpha, and carbon energy loss when they pass through the glass system. As shown in Fig. 8(a), ESP values drop as kinetic energy increases.

Moreover, the ES_P values drop with increasing Gd_2O_3 concentration, with the lowest AS_P values found in the ZABSG5 glass system. As presented in Fig. 8(b), maximum PS_P values are reached at a kinetic energy of 0.080 MeV and then drop when the kinetic energy increases. Furthermore, The PS_P values decrease with the increase in Gd_2O_3 concentration. The ZABSG5 glass system has the lowest PMSP values in kinetic energy. Figure 8(c), when the kinetic energy increases to a maximum of 0.8 MeV, AMSP values increase, and in case of increasing the kinetic energy values, the AMSP values decrease.

Furthermore, The AS_P values decrease with the increase in Gd_2O_3 concentration. The prepared ZABSG5 glass system has the lowest AS_P values in the kinetic energy range of 0.015–15 MeV. Figure 8(d) shows that the CS_P values increase to a kinetic energy of about 5 MeV, then fall when the kinetic energy is increased further. In addition, in the kinetic energy range of 0.015–15 MeV, the CS_P values are lowest for the ZABSG5 glass system, which decreases as Gd_2O_3 concentration increases. ZABSG5 glass has the greatest density (4.109 g.cm^{-3}) and the highest content of high atomic number (Gd = 64), which may account for these characteristics.

The fast neutrons removal cross section shows the probability that neutrons will pass through a substance without reacting (Σ_R, cm^{-1}). As seen in Fig. 9(a, b), The Σ_R of the studied samples have values of 0.1076, 0.1090, 0.1094, 0.1103, and 0.1111 cm^{-1} for ZABSG1, ZABSG2, ZABSG3, ZABSG4 and ZABSG5 respectively. ZABSG5 has the highest value of the $\Sigma_{R,}$ and ZABSG1 has the lowest due to the concentration of gadolinium (Gd) element used in fuel assemblies as a neutron absorber. Also, the prepared samples' thermal neutrons cross section (σ_{tot}, cm^{-1}) were calculated. The σ_{tot} of the studied glass samples have the same behavior. The σ_{tot} of the prepared glass samples have 38.4298, 45.5252, 52.3455, 66.3203, and 80.5895 for ZABSG1, ZABSG2, ZABSG3, ZABSG4 and ZABSG5 respectively. ZABSG5 has the highest value of the $\sigma_{tot,}$ and ZABSG1 has the lowest, as listed in Table 3. Therefore, we may deduce that Gd element doping gives the studied compound a high potential across the neutrons shielding Table 4.

Table 4 Coherent scattering cross-section (σ_{coh}), incoherent scattering cross-section (σ_{inc}), absorption cross-section (σ_{abs}), and total cross-section (σ_{tot}) of the prepared ZnO–Al_2O_3–B_2O_3–SiO_2-Gd_2O_3 glasses for thermal neutrons attenuation

Sample code	Thermal neutron cross section (cm^{-1})			
	σ_{coh}	σ_{inc}	σ_{abs}	σ_{tot}
ZABSG1	0.95991	0.08416	37.38575	38.42982
ZABSG2	0.98389	0.10507	44.43632	45.52528
ZABSG3	0.99874	0.12546	51.22135	52.34555
ZABSG4	1.02958	0.16721	65.12357	66.32036
ZABSG5	1.05953	0.20990	79.32015	80.58958

4 Conclusion

This research reported on the shielding qualities of xGd_2O_3 – (60-x)ZnO–$15B_2O_3$–$5Al_2O_3$–$20SiO_2$ glass system (x = 0—3 mol %) for gamma photon starting from 15 keV up to 15 MeV. The results of the μ_m obtained from FLUKA and XCOM show a good agreement with a maximum relative difference of 0.901%. Also, the μ_m values, in the unit of $cm^2.g^{-1}$, for the investigated system were varied from 43.2341 to 0.0264 for ZABSG1, 43.918 to 0.02684 for ZABSG2, 44.6005 to 0.0272 for ZABSG3, 45.9117 to 0.0280 for ZABSG4 and 47.1887 to 0.0287 for ZABSG5 in the energy range of 0.015 – 15 MeV. Also, The FNRCS values were 0.1076, 0.1090, 0.1094, 0.1103, and 0.1111 cm^{-1} for ZABSG1, ZABSG2, ZABSG3, ZABSG4, and ZABSG5 respectively. In addition, The TNRCS values were 38.4298, 45.5252, 52.3455, 66.3203, and 80.5895 for ZABSG1, ZABSG2, ZABSG3, ZABSG4, and ZABSG5 respectively. The glass sample ZABSG5 had the highest values of μ_m, μ, and T/FNRCS and the lowest values of HVL and ƛ due to the high concentration of Gd_2O_3 (11.122%) and density (4.109 g.cm^{-3}) and Z_{eff}. The results referred to the high radiation shielding potential for the present glassy materials as compared with previously studied shielding materials, which should aid in developing effective radiation shielding materials for use in the nuclear and medical industries.

Acknowledgements The authors express their gratitude to Princess Nourah bint Abdulrahman University Researchers Supporting Project number (PNURSP2023R291), Princess Nourah bint Abdulrahman University, Riyadh, Saudi Arabia.

Author Contributions Writing the first draft of the manuscript and reviewing-editing were performed by Nada Alfryyan, Z.A. Alrowaili, Sultan Alomairy, Islam M. Nabil, and M.S. Al-Buriahi. All authors reviewed the manuscript.

Funding The authors express their gratitude to Princess Nourah bint Abdulrahman University Researchers Supporting Project number (PNURSP2023R291), Princess Nourah bint Abdulrahman University, Riyadh, Saudi Arabia.

Data Availability The data that support the findings of this study are available from the corresponding author upon reasonable request.

Code Availability Not applicable.

Declarations

Ethics Approval Not applicable.

Consent to Participate Not applicable.

Consent for Publication Not applicable.

Competing Interests The authors declare no competing interests.

References

1. Mettler Jr FA, Guiberteau MJ (2012) Essentials of nuclear medicine imaging: expert consult-online and print. Elsevier Health Sciences
2. Hegazy HH, Al-Buriahi MS, Alresheedi F, Alraddadi S, Arslan H, Algarni H (2021) The effects of TeO_2 on polarizability, optical transmission, and photon/neutron attenuation properties of boro-zinc-tellurite glasses. J Inorg Organomet Polym Mater 31:2331–2338
3. Hegazy HH, Al-Buriahi MS, Alresheedi F, El-Agawany FI, Sriwunkum C, Neffati R, Rammah YS (2021) Nuclear shielding properties of B2O3–Bi2O3–SrO glasses modified with Nd2O3: theoretical and simulation studies. Ceram Int 47(2):2772–2780
4. Boukhris I, Kebaili I, Al-Buriahi MS, Alalawi A, Abouhaswa AS, Tonguc B (2020) Photon and electron attenuation parameters of phosphate and borate bioactive glasses by using Geant4 simulations. Ceram Int 46(15):24435–24442
5. Lakshminarayana G, Kebaili I, Dong MG, Al-Buriahi MS, Dahshan A IV, Kityk D-E Lee, Yoon J, Park T (2020) Estimation of gamma-rays, and fast and the thermal neutrons attenuation characteristics for bismuth tellurite and bismuth boro-tellurite glass systems. J Mater Sci 55:5750–5771
6. Divina R, Naseer KA, Marimuthu K, Alajerami YSM, Al-Buriahi MS (2020) Effect of different modifier oxides on the synthesis, structural, optical, and gamma/beta shielding properties of bismuth lead borate glasses doped with europium. J Mater Sci Mater Electron 31:21486–21501
7. Rammah YS, Tekin HO, Sriwunkum C, Olarinoye I, Alalawi A, Al-Buriahi MS, Nutaro T, Tonguc BT (2021) Investigations on borate glasses within SBC-Bx system for gamma-ray shielding applications. Nucl Eng Technol 53(1):282–293
8. Sayyed MI, Laariedh F, Kumr A, Al-Buriahi MS (2020) Experimental studies on the gamma photons-shielding competence of TeO_2–PbO–BaO–Na_2O–B_2O_3 glasses. Appl Phys A 126:1–9
9. Alothman MA, Alrowaili ZA, Alzahrani JS, Abdel Wahab EA, Olarinoye IO, Sriwunkum C, Shaaban KS, Al-Buriahi MS (2021) Significant influence of MoO_3 content on synthesis, mechanical, and radiation shielding properties of B_2O_3-Pb_3O_4-Al_2O_3 glasses. J Alloys Compd 882:160625
10. Bashter I (1997) Calculation of radiation attenuation coefficients for shielding concretes. Ann Nucl Energy 24(17):1389–1401
11. Al-Buriahi MS, Gaikwad DK, Hegazy HH, Sriwunkum C, Neffati R (2021) Fe-based alloys and their shielding properties against directly and indirectly ionizing radiation by using FLUKA simulations. Physica Scripta 96(4):045303
12. Alzahrani JS, Alrowaili ZA, Eke C, Mahmoud ZMM, Mutuwong C, Al-Buriahi MS (2022) Nuclear shielding properties of Ni-, Fe-, Pb-, and W-based alloys. Radiat Phys Chem 195:110090
13. Al-Buriahi MS, Singh VP, Arslan H, Awasarmol VV, Tonguc BT (2020) Gamma-ray attenuation properties of some NLO materials: potential use in dosimetry. Radiat Environ Biophys 59(1):145–150
14. Lakshminarayana G, Dong MG, Al-Buriahi MS, Kumar A, Lee D-E, Yoon J, Park T (2020) B_2O_3–Bi_2O_3–TeO_2–BaO and TeO_2–Bi_2O_3–BaO glass systems: A comparative assessment of gamma-ray and fast and thermal neutron attenuation aspects. Appl Phys A 126:1–18
15. Mhareb MHA, Alajerami YSM, Dwaikat N, Al-Buriahi MS, Alqahtani M, Alshahri F, Saleh N, Alonizan N, Saleh MA, Sayyed MI (2021) Investigation of photon, neutron and proton shielding features of H_3BO_3–ZnO–Na_2O–BaO glass system. Nucl Eng Technol 53(3):949–959
16. Alothman MA, Olarinoye IO, Sriwunkum C, Alomairy S, Alzahrani JS, Al-Buriahi MS (2022) Study of the radiation attenuation properties of MgO-Al2O3-SiO2-Li2O-Na2O glass system. J Aust Ceram Soc. Springer, p 1–7
17. Lakshminarayana G, Kumar A, Tekin HO, Issa SAM, Al-Buriahi MS, Lee D-E, Yoon J, Park T (2020) Binary B_2O_3–Bi_2O_3 glasses: scrutinization of directly and indirectly ionizing radiations shielding abilities. J Mater Res Technol 9(6):14549–14567
18. Al-Buriahi MS, Eke C, Alomairy S, Mutuwong C, Sfina N (2021) Micro-hardness and gamma-ray attenuation properties of lead iron phosphate glasses. J Mater Sci Mater Electron 32(10):13906–13916
19. Alzahrani JS, Sharma A, Nazrin SN, Alrowaili ZA, Al-Buriahi MS (2022) Optical and radiation shielding effectiveness of a newly fabricated WO_3 doped TeO_2–B_2O_3 glass system. Radiat Phys Chem 193:109968
20. Al-Buriahi MS, Olarinoye IO, Alomairy S, Kebaili I, Kaya R, Arslan H, Tonguc BT (2021) Dense and environment friendly bismuth barium telluroborate glasses for nuclear protection applications. Prog Nucl Energy 137:103763
21. Kilic G, Ilik E, Issa SAM, Issa B, Al-Buriahi MS, Issever UG, Zakaly HMH, Tekin HO (2021) Ytterbium (III) oxide reinforced novel TeO_2–B_2O_3–V_2O_5 glass system: Synthesis and optical, structural, physical and thermal properties. Ceram Int 47(13):18517–18531
22. Al-Buriahi MS, Arslan H, Tekin HO, Singh VP, Tonguc BT (2020) MoO_3-TeO_2 glass system for gamma ray shielding applications. Mater Res Express 7(2):025202
23. Al-Buriahi MS, Gaikwad DK, Hegazy HH, Sriwunkum C, Algarni H (2021) Newly developed glasses containing Si/Cd/Li/Gd and their high performance for radiation applications: role of Er_2O_3. J Mater Sci Mater Electron 32:9440–9451
24. Kebaili I, Znaidia S, Alzahrani JS, Alothman MA, Boukhris I, Olarinoye IO, Mutuwong C, Al-Buriahi MS (2021) Ge20Se80-xBix ($x \leq 12$) chalcogenide glasses for infrared and gamma sensing applications: structural, optical and gamma attenuation aspects. J Mater Sci Mater Electron 32(11):15509–15522
25. Al-Hadeethi Y, Sayyed MI, Al-Buriahi MS (2020) Bioactive glasses doped with TiO_2 and their potential use in radiation shielding applications. Ceram Int 46(10):14721–14732
26. Halimah MK, Eevon C (2019) Comprehensive study on the effect of Gd2O3 NPs on elastic properties of zinc borotellurite glass system using non-destructive ultrasonic technique. J Non-Cryst Solids 511:10–18
27. Morshidy HY, Abd El-Fattah ZM, Abul-Magd A, Hassan MA, Mohamed AR (2021) Reevaluation of Cr6+ optical transitions through Gd2O3 doping of chromium-borate glasses. Opt Mater 113:110881
28 Al-Buriahi MS, Tonguç B, Perişanoğlu U, Kavaz E (2020) The impact of Gd2O3 on nuclear safety proficiencies of TeO_2–ZnO–Nb_2O_5 glasses: a GEANT4 Monte Carlo study. Ceram Int 46(15):23347–23356
29 Al-Hadeethi Y, Sayyed MI (2020) Effect of Gd2O3 on the radiation shielding characteristics of Sb_2O_3–PbO–B_2O_3–Gd_2O_3 glass system. Ceram Int 46(9):13768–13773
30. Ismail NAN, Zaid MHM, Matori KA, Fen YW, Cheong WM, Loh ZW, Shah AZ, Hisam R, Azlan MN, Iskandar SM (2023)

Role of Gd_2O_3 on structure rearrangement and elastic properties $ZnO\text{-}Al_2O_3\text{-}B_2O_3\text{-}SiO_2$ glass system. Optik 276:170659
31. Berger MJ, Hubbell JH (1987) XCOM: Photon cross sections on a personal computer. No. NBSIR-87–3597. National Bureau of Standards, Washington, DC (USA). Center for Radiation Research
32. Al-Buriahi MS, Alrowaili ZA, Alsufyani SJ, Olarinoye IO, Alharbi AN, Sriwunkum C, Kebaili I (2022) The role of PbF_2 on the gamma-ray photon, charged particles, and neutron shielding prowess of novel lead fluoro bismuth borate glasses. J Mater Sci Mater Electron 33(3):1123–1139
33. Al-Buriahi MS, Alzahrani JS, Olarinoye IO, Akyildirim H, Alomairy S, Kebaili I, Tekin HO, Mutuwong C (2021) Role of heavy metal oxides on the radiation attenuation properties of newly developed TBBE-X glasses by computational methods. Physica Scripta 96(7):075302
34 Sekhar KC, Narsimlu N, Al-Buriahi MS, Yakout HA, Olarinoye IO, Alomairy S, Shareefuddin MD (2021) Synthesis, optical, and radiation attenuation properties of $CaF_2\text{-}TeO_2\text{-}Na_2B_4O_7\text{-}CuO$ glass system for advanced shielding applications. Eur Phys J Plus 136(9):903
35. Al-Buriahi MS (2023) Radiation shielding performance of a borate-based glass system doped with bismuth oxide. Radiat Phys Chem 207:110875
36. Khattari ZY, Al-Buriahi MS (2022) Monte Carlo simulations and Phy-X/PSD study of radiation shielding effectiveness and elastic properties of barium zinc aluminoborosilicate glasses. Radiat Phys Chem 195:110091
37. Alharshan GA, Alrowaili ZA, Olarinoye IO, Al-Buriahi MS (2022) Holmium (III) oxide and its significant effects on the radiation shielding performance of P2O5+ B2O3+ ZnSO4 optical glasses. Optik 261:169188
38. Alharshan GA, Alrowaili ZA, Olarinoye IO, Sriwunkum C, Tonguc BT, Al-Buriahi MS (2022) Optical borophosphate glass system with excellent properties for radiation shielding applications. Optik 266:169568
39. Alothman MA, Alrowaili ZA, Al-Baradi AM, Kilicoglu O, Mutuwong C, Al-Buriahi MS (2021) Elastic properties and radiation shielding ability of ZnO–P2O5/B2O3 glass system. J Mater Sci Mater Electron 32(14):19203–19217
40. Al-Buriahi MS, Taha TA, Alothman MA, Donya H, Olarinoye IO (2021) Influence of WO3 incorporation on synthesis, optical, elastic and radiation shielding properties of borosilicate glass system. Eur Phys J Plus 136(7):779
41. Al-Buriahi MS, Eke C, Alomairy S, Yildirim A, Alsaeedy HI, Sriwunkum C (2021) Radiation attenuation properties of some commercial polymers for advanced shielding applications at low energies. Polym Adv Technol 32:2386–2396
42. Al-Buriahi MS, Sriwunkum C, Boukhris I (2021) X- and gamma-rays attenuation properties of DNA nucleobases by using FLUKA simulation code. Eur Phys J Plus 136:776
43 Saeed A, Alomairy S, Sriwunkum C, Al-Buriahi MS (2021) Neutron and charged particle attenuation properties of volcanic rocks. Radiat Phys Chem 184:109454
44. Alshahrani B, Olarinoye IO, Mutuwong C, Sriwunkum C, Yakout HA, Tekin HO, Al-Buriahi MS (2021) Amorphous alloys with high Fe content for radiation shielding applications. Radiat Phys Chem 183:109386
45. Alalawi A, Al-Buriahi MS, Sayyed MI, Akyildirim H, Arslan H, Zaid MHM, Tonguç BT (2020) Influence of lead and zinc oxides on the radiation shielding properties of tellurite glass systems. Ceram Int 46(11):17300–17306